Simulation study of halo formation in breathing round beams

Hiromi Okamoto and Masanori Ikegami
Accelerator Laboratory, Institute for Chemical Research, Kyoto University, Gokanoshou, Uji, Kyoto 611, Japan
(Received 19 August 1996; revised manuscript received 17 January 1997)

We study halo formation from cylindrical beams propagating in a uniform focusing channel. Of particular interest here are the breathing-mode oscillations excited by an initial beam-size mismatch. We develop a one-dimensional space-charge code which is simple but powerful in exploring the halo properties of breathing beams. After giving a brief description of two particle-core models, we apply the developed code to three different types of nonlinear phase-space distributions. Based on a number of multiparticle simulation runs, we show several interesting results useful for the design considerations of high-power linear machines. In particular, the intensity of halo current as well as the maximum extent of halos are self-consistently evaluated with the different sizes of initial mismatch and beam density. We then find that the halo extent normalized with the initial root-mean-squared beam size is only weakly dependent on the tune depression and that the halo intensity appears to increase with the degree of mismatch. It is further demonstrated that the beam core in phase space is roughly stable and, thus, most halo particles remain outside the core boundary. We also see that it is, in principle, possible to scrape halos, e.g., by means of a multicollimator system. [S1063-651X(97)09304-5]

PACS number(s): 29.27.Eg, 07.77.−n, 41.75.−i, 52.25.Wz

I. INTRODUCTION

In designing a linac system for intense beam acceleration, it is extremely important to have a clear understanding of space-charge effects since the beam quality can easily be deteriorated by them. Though much effort has so far been devoted to studying space-charge-induced phenomena, there still exist some unsolved problems which must be investigated in more detail. The mechanism of halo formation is one such problem [1]. In fact, recent interest in using high-current ion linacs for the production of tritium, the transmutation of nuclear waste, etc. has greatly enhanced the activity of halo study, because these machines must operate with a very low beam loss to avoid serious radio activation [2,3].

Through extensive simulation works, it is now commonly believed that a key mechanism responsible for halo generation is parametric resonances excited by the plasma oscillation of a dense beam core [4]. Based on this idea, a variety of theoretical and numerical calculations have been performed to establish a quantitative description of the halo formation process. A popular strategy for this purpose is, for example, the use of the so-called *particle-core model* which was first suggested by Gluckstern in an unpublished paper [5] and was further developed by other researchers [6–8]. In this model, we usually take into account a Kapchinskij-Vladimirskij (KV) core [9] executing the lowest-order breathing oscillation. Then, the motion of a test particle driven by the oscillating core potential is analyzed, assuming that the core distribution is not affected by the existence of the test particle.

It is an easy matter to show that, because of the stability of the core oscillation mode [10], the particle-core model never provides an explanation as to why a fraction of beam particles can escape from the core region, forming a halo. We may, however, recall that a realistic beam always involves some particles around the core as the tail. For these tail particles, this model might turn to a useful tool, since the homogenization effect [11] makes the real-space distribution of any dense core nearly uniform and, accordingly, the space-charge field acting upon the tail particles becomes similar to that generated by a KV core [12]. The particle-core model could, thus, give us good insight into halo dynamics, and should be worthwhile to pursue.

Another approach frequently employed for halo study is based on root-mean-squared (rms) quantities. The envelope equation [13] is taken, under the assumption of invariant rms emittance, to reconsider the resonant instability caused by the periodicity of a focusing channel [14,15]. From the viewpoint that the periodic change of external restoring force gives rise to the instability, this effect may be regarded as the well-known *structure-driven resonances*, which had not been linked to beam halo problems until recently. The rms approach has a major advantage that the envelope equation is independent of particle distribution unless the corresponding real-space density breaks an elliptical symmetry. The constant-emittance assumption is, however, inconsistent with the halo formation process and, further, the system periodicity is not necessarily required to have halos generated. It is thus presently uncertain how accurately this model describes the essence of halo properties. Further investigations, in particular, a careful comparison with self-consistent simulation results would be needed to confirm its validity.

In this paper, we show systematic self-consistent simulation results to deepen our current understandings of halo formation in a uniform focusing channel; where no structure-driven resonances can be excited. We develop here a multiparticle code dedicated to a breathing-mode study since we are especially interested in the core oscillations caused by an initial beam-size mismatch. The beams considered in the following sections are thus kept strictly round throughout the channel. In this case, the usual time-consuming two-dimensional (2D) particle-in-cell (PIC) algorithm becomes unnecessary because of the symmetry of the problem. In addition, the accuracy of the present space-charge calculations should probably be higher than that of 2D PIC calculations, since we only need 1D meshes and, consequently, a large

number of simulation particles are usable with less CPU time.

The paper is organized as follows. We first give a brief review of the particle-core model in Sec. II for the sake of completeness. In addition to the ordinary KV-based analysis, an alternate algorithm with a waterbag core is presented [21]. The 1D simulation procedure for breathing modes is then described in Sec. III. In Sec. IV, the developed code is applied to several different types of initial phase-space distributions in order to examine their stability properties. In Sec. V, we try to draw, based on the present simulation results, some practical criteria useful for a linac design. Finally, the obtained results are summarized in Sec. VI.

II. PARTICLE-CORE MODEL

A. The KV model

The first basis of the particle-core analysis is the envelope equation given by

$$\frac{d^2a}{dz^2}+\kappa^2 a=\frac{K}{2(a+b)}+\frac{(\varepsilon^x_{\rm rms})^2}{16a^3}, \tag{2.1}$$

where a and b are, respectively, the rms beam size of the horizontal and vertical direction, κ is the constant parameter related to the betatron tune in the absence of space charge, K is the beam perveance, and $\varepsilon^x_{\rm rms}$ is the rms emittance of the horizontal motion. A similar equation holds for the vertical motion. Specifically, $a=b$ and $\varepsilon^x_{\rm rms}=\varepsilon^y_{\rm rms}\equiv\varepsilon$ for breathing oscillations. Equation (2.1) can then be simplified to

$$\frac{d^2\rho}{d\tau^2}+\rho=\frac{\Gamma}{2\rho}+\frac{1}{4\rho^3}, \tag{2.2}$$

where $\rho=\sqrt{2\kappa/\varepsilon}a=\sqrt{2\kappa/\varepsilon}b$, $\Gamma=K/\kappa\varepsilon$, and $\tau=\kappa z$. The parameter Γ can be related to the tune depression η, i.e., the ratio of the space-charge depressed betatron frequency to the zero-current frequency κ, as

$$\Gamma=\frac{1-\eta^2}{\eta}. \tag{2.3}$$

Let us now introduce the convenient dimensionless canonical variables defined by $\tilde{r}=\sqrt{\kappa/\varepsilon}r$, $\tilde{\theta}=\theta$, $\tilde{p}_r=p_r/\sqrt{\kappa\varepsilon}$, and $\tilde{p}_\theta=p_\theta/\varepsilon$, where (r,θ) denote polar coordinates and (p_r,p_θ) are the conjugate momenta. The independent variable in this scaled system is τ. The angular momentum p_θ is a constant of motion in breathing round beams, i.e., $\tilde{p}_\theta\equiv L=$const, since the angle coordinate θ is cyclic. Then, assuming a KV core executing the lowest-order mode oscillation, the equation of test-particle motion can be written as

$$\frac{d^2r}{d\tau^2}+r-\frac{L^2}{r^3}=\begin{cases}\dfrac{\Gamma}{R^2}r & (r\leqslant R)\\[2ex] \dfrac{\Gamma}{r} & (r>R),\end{cases} \tag{2.4}$$

which is the second basis of the particle-core analysis. Here, the beam has the clear circular boundary whose scaled radius is $R(\tau)=\sqrt{2}\rho=\sqrt{\kappa/\varepsilon}2a$, and the tilde has been dropped. In the rest of this paper, we always employ the scaled variables without indicating the tilde.

As pointed out previously [5], the particle-core resonance becomes most predominant when $L=0$. We, therefore, consider the simpler equation

$$\frac{d^2x}{d\tau^2}+x=\begin{cases}\dfrac{\Gamma}{R^2}x & (|x|\leqslant R)\\[2ex] \dfrac{\Gamma}{x} & (|x|>R),\end{cases} \tag{2.5}$$

instead of Eq. (2.4). In the particle-core algorithm, we first numerically integrate Eq. (2.2) with the initial conditions, e.g., $\rho(\tau=0)=\mu\rho_0$ and $(d\rho/d\tau)(\tau=0)=0$, where μ is mismatch factor [16], and the matched beam size ρ_0 can be evaluated from

$$\rho_0^2=\frac{\Gamma+\sqrt{\Gamma^2+4}}{4}. \tag{2.6}$$

The result is then substituted in Eq. (2.5) to determine the time evolution of the coordinate x. It is important to note that Γ is the only parameter involved in the particle-core system.

As long as we assume that the real-space density is kept uniform even in a mismatched beam, the set of the particle-core equations, i.e., Eqs. (2.2) and (2.4), is self-consistent due to the linearity of the mode. This suggests that we have no chance in this model to observe halos, because halo formation is generally accompanied by the emittance growth contradictory to the self-consistency of this system. However, once we initially have some particles outside the core, they will readily be trapped by resonances acquiring large amplitudes. The trajectories of these particles may be determined, to a good approximation, with the particle-core analysis, since any realistic dense core possesses an almost uniform distribution in real space and, thus, the resulting space-charge field resembles that of a KV beam except in the vicinity of the core boundary [17].

B. A waterbag model

KV distribution has frequently been taken as a theoretical basis of space-charge study because its linearity considerably simplifies analyses. However, there is no doubt that realistic intense beams contain a fully nonlinear nature. It may thus be reasonable to try constructing an alternate particle-core algorithm with a nonlinear core potential even if the model is only approximate. From this point of view, we introduce here a waterbag core under a simplifying assumption.

Let us first start from the stationary waterbag density

$$n_0(r)=\frac{N}{\pi\Gamma}\left[1-\frac{I_0(\zeta_0 r)}{I_0(\zeta_0 P_0)}\right], \tag{2.7}$$

where $I_n(z)$ denotes the modified Bessel function of the nth order, P_0 is the scaled radius of the matched waterbag-beam boundary, N is the total number of ions, and ζ_0 is the constant satisfying

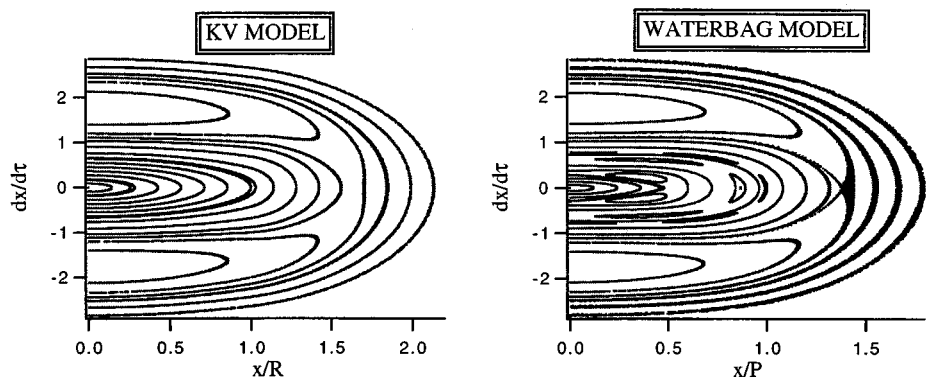

FIG. 1. Poincaré surfaces of section in the $(x, dx/d\tau)$ phase space. The left figure is based on the KV model and the right one on the waterbag model. The conditions that $\eta=0.5$ and $\mu=1.1$ have been assumed in both cases.

$$\frac{\Gamma}{P_0^2}\frac{I_0(\zeta_0 P_0)}{I_2(\zeta_0 P_0)}=1. \tag{2.8}$$

Assuming that the waterbag-type density is roughly maintained even for a mismatched beam, we may replace P_0 and ζ_0 in Eq. (2.7) by $P(\tau)$ and $\zeta(\tau)$ which represent, respectively, the boundary size of the mismatched waterbag core and the variable satisfying the relation analogous to Eq. (2.8), i.e.,

$$\frac{\Gamma}{P^2}\frac{I_0(\zeta P)}{I_2(\zeta P)}=1. \tag{2.9}$$

The equation of motion for a test particle with $L=0$ is then given by

$$\frac{d^2x}{d\tau^2}+x=\begin{cases} x-\dfrac{2I_1(\zeta x)}{\zeta I_0(\zeta P)} & (|x|\leqslant P) \\ \dfrac{\Gamma}{x} & (|x|>P). \end{cases} \tag{2.10}$$

To make a physically meaningful comparison between results from the KV model and those from the waterbag model, the two beam cores must be so-called equivalent; namely, the second moments of both beams in a matched state must coincide with each other. Needless to say, the values of η and μ are taken to be the same in both models. $P(\tau)$ and $\zeta(\tau)$ can be found by solving Eq. (2.9) together with the relation

$$\rho^2=\frac{4}{\zeta^2}+P^2-\frac{P^4}{2\Gamma} \tag{2.11}$$

in which we are allowed to use the envelope function $\rho(\tau)$ identical to that already obtained in the KV-model analysis, because $\rho(\tau)$ is independent of beam distributions in our case. Finally, the time evolution of $P(\tau)$ and $\zeta(\tau)$ are substituted in Eq. (2.10) to investigate the single-particle motion.

C. Numerical results

For a systematic study of halo dynamics, it is convenient to employ the *Poincaré mapping technique* first introduced to the particle-core approach by Lagniel [7]. As an example, we show, in Fig. 1, the Poincaré surfaces of section obtained with $\eta=0.5$ and $\mu=1.1$ [18]. Not surprisingly, both pictures look quite similar in the region outside the core separatorices. On the other hand, the inside of the waterbag core is more complicated, exhibiting some higher-order islands which can never be found in the KV core at any density. Further, the core separatrix of the waterbag beam is no longer elliptic as seen in the KV case, but has been distorted to be a racetrack shape due to the core nonlinearity.

In a higher-density region, the waterbag core begins to show an even more interesting feature substantially different from the KV core. Figure 2(a) illustrates the Poincaré surface of the section corresponding to a mismatched KV beam with $\eta=0.2$. Naturally, the inside of the core is still completely regular. Contrarily, as demonstrated in Fig. 2(b), the regularity of the waterbag core with the same η and μ has collapsed, yielding a large stochastic domain around a certain core boundary. Considering the nonlinear nature of a realistic beam, there is no reason to deny the possibility of such a stochastic instability of the core tail which could somewhat enhance the halo intensity. Note further that, in this model,

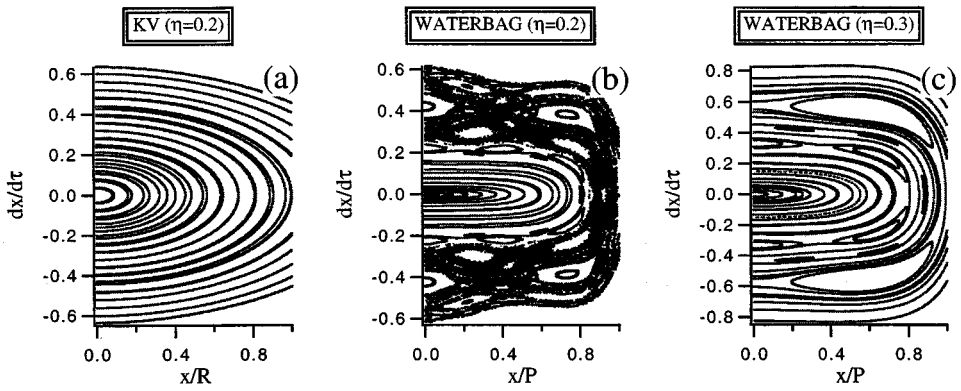

FIG. 2. Poincaré surfaces of section in the $(x, dx/d\tau)$ phase space. (a) KV beam with $\eta=0.2$ and $\mu=1.01$, (b) waterbag beam with $\eta=0.2$ and $\mu=1.01$, and (c) waterbag beam with $\eta=0.3$ and $\mu=1.01$.

the transition to this major chaos takes place in the region between $\eta=0.2$ and $\eta=0.3$. In fact, we can only observe very thin layers of stochasticity in Fig. 2(c) where $\eta=0.3$ has been assumed.

III. SIMULATION METHOD

We now describe a 1D simulation method for breathing beams. Because of the symmetry of breathing modes, the Hamiltonian governing the system of our interest is independent of the angle coordinate θ even for mismatched beams. The azimuthal motion of each particle is then a simple rotation with the constant angular momentum $p_\theta=L$, which means that we do not have to care about the azimuthal dynamics. The equation of the radial motion can thus be written in a closed form as

$$\frac{d^2r}{d\tau^2}+r-\frac{L^2}{r^3}=\frac{2\pi\varepsilon_0\Gamma}{Nq}E_r(r;\tau), \tag{3.1}$$

where q is the charge state of a single ion, E_r is the scaled radial component of the space-charge electric field depending on r and τ, and the constant L takes different values for different particles. E_r can readily be obtained, according to Gauss's law, as

$$E_r(r;\tau)=\frac{Q(r;\tau)}{2\pi\varepsilon_0 r}, \tag{3.2}$$

where $Q(r;\tau)$ represent the total charge contained in the circular region of the radius r; namely, $Q(r;\tau)=q\int_0^r dr\int_{-\infty}^{+\infty}dp_r f(r,p_r;\tau)$ with $f(r,p_r;\tau)$ being the distribution function in the (r,p_r) phase space. Hence, all we have to do to evaluate E_r at $r=r_0$ is simply count the number of ions located in the region $r<r_0$ at a given time. Finally, substitution of Eq. (3.2) into Eq. (3.1) yields the equation of motion

$$\frac{d^2r}{d\tau^2}+r-\frac{L^2}{r^3}=\Gamma\frac{\xi(r;\tau)}{r}, \tag{3.3}$$

where $\xi(r;\tau)=Q(r;\tau)/Nq$. To determine the time evolution of the particle distribution, we here apply the second- or fourth-order symplectic integrator to Eq. (3.3), fixing the function $\xi(r;\tau)$ within each time step. Moreover, we have adopted the variable step-size scheme to improve the accuracy of the numerical integration.

It is evident from Eq. (3.3) that the free parameters which must be given initially are only two; namely, the mismatch factor μ and the space-charge factor Γ. The particle-dependent constant L can be obtained from the relation $L=xp_y-yp_x$ once an initial distribution is generated in four-dimensional phase space. The matched rms beam size ρ_0 is calculated with Eq. (2.6). Noting Eq. (2.3), we may also say that, except for the mismatch factor μ, the tune depression η is the only parameter necessary for the execution of this simulation procedure.

For later convenience, we here express the plasma wave length λ_p by means of η. Taking the conventional definition of plasma frequency, e.g., Eq. (4) in Ref. [10], it is straightforward to show the relation

$$\lambda_p=\frac{2\pi}{\kappa\sqrt{1-\eta^2}}. \tag{3.4}$$

Recalling that the independent variable we have adopted is $\tau=\kappa z$, the scaled plasma wave length $\tau_p=\kappa\lambda_p$ again depends only on η.

In order to figure out the adequate values of the simulation parameters, such as the number of particles, the size of integration step, etc., we performed preliminary runs employing Gaussian beams. We then found that the results were insensitive to the radial mesh size provided that more than 100 meshes were taken over the length ρ_0. Regarding the particle number, only little change was observed between results with 10^4 particles and those with 10^5 particles. We, therefore, decided to employ 10^4 particles for the sake of reducing computing time. As to the integration step size, we tried three cases, i.e., 2^{10} steps, 2^{11} steps, and 2^{12} steps over the characteristic length τ_p, and again obtained good agreements among the three outputs. To be on the safer side, we chose 2^{11} steps per τ_p. Note, however, that this number corresponds to the largest step size. As mentioned above, we have used the variable step-size algorithm, monitoring the energy change of each particle in every integration step. The possible finest step size which may occur in our code has been set to be $\tau_p/2^{25}$.

We also calculated the value of the quantity $\langle\xi\rangle$, where $\langle\xi\rangle$ stands for taking the average of ξ over the whole phase space. Since straightforward algebra reveals the fact that $\langle\xi\rangle$ is exactly equal to 0.5 independent of beam distribution, we can use this quantity to check the accuracy of our numerical calculations. With the parameter setup determined above, $\langle\xi\rangle$ oscillates about 0.5 with the amplitude less than 0.001, which suggests that our code possesses a sufficient accuracy. Finally, we compared solutions to the envelope equation with simulation results. Due to the independence of the envelope equation on beam distributions as well as to the symmetry of breathing beams, the time evolution of the rms beam size obtained from a simulation must exactly coincide with the numerical solution to Eq. (2.1) provided that the corresponding time evolution of the rms emittance is used for $\varepsilon^x_{\rm rms}$ in Eq. (2.1). In fact, we always got perfect agreement between them.

IV. STABILITY OF BREATHING BEAMS

The best way to overcome the limitations of approximate analytic approaches is to perform multiparticle simulations which enable us to self-consistently explore the fundamental properties of dense beams. In order for our simulation results to be practically meaningful, we should let an input beam have some sufficiently realistic distribution. Since, in practice, the initial phase-space distribution of a beam injected into a linac depends on various components, such as the beam source, the short matching section between the source, and the linac, etc., we treat, in the following, three different types of nonlinear distributions; namely, Gaussian-, waterbag-, and parabolic-type distributions. There is no doubt that these distributions are more stable and realistic, at least, than the KV distribution and are thus adequate to our purpose.

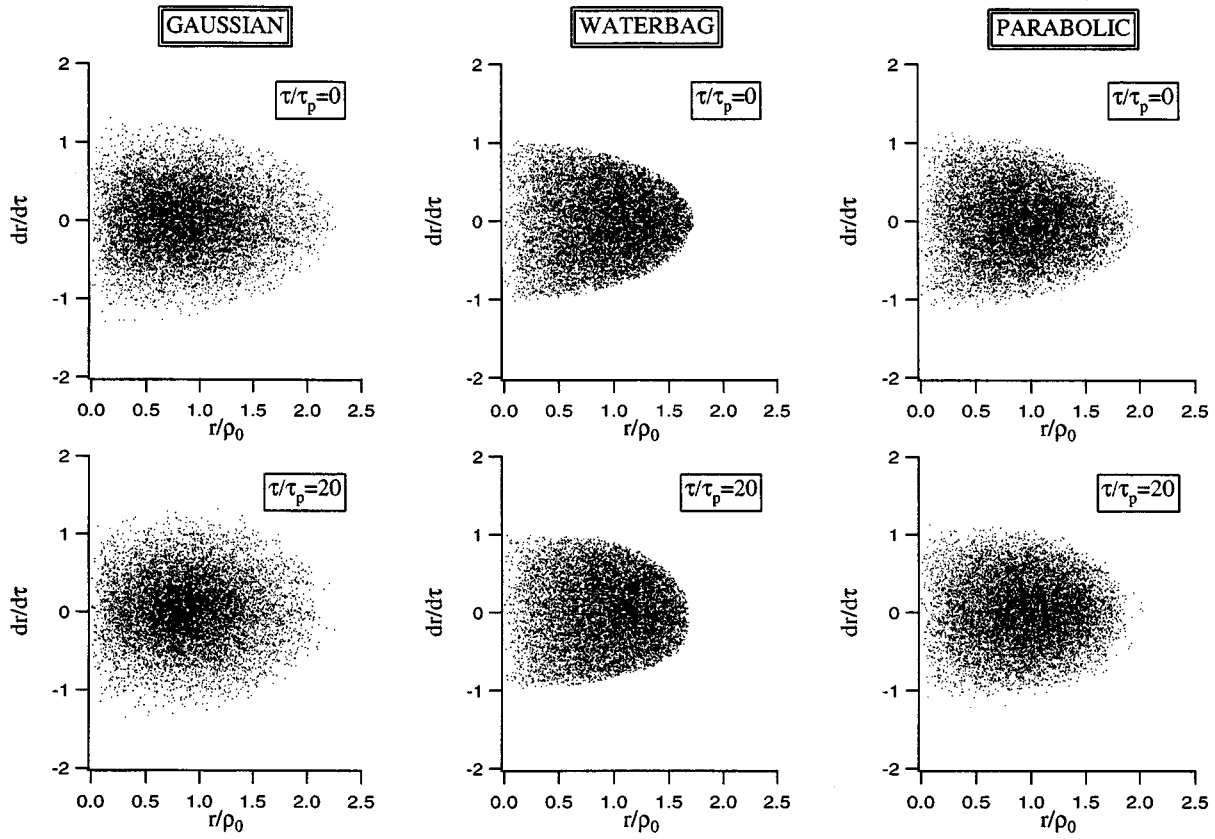

FIG. 3. Phase-space configurations of rms-matched beams with $\eta=0.7$ at $\tau/\tau_p=0$ and $\tau/\tau_p=20$.

Let us first consider the beams initially rms matched. Figure 3 illustrates the phase-space configurations of the three beams with the tune depression of 0.7. The upper pictures correspond to the initial distributions while the lower ones to the distributions at $\tau/\tau_p=20$. Slight core distortion due to the weak density redistribution [19] can be observed in each case, but all beams look stable in this density region, as anticipated. In fact, almost no emittance growth was detected. In the $\eta=0.3$ case shown in Fig. 4, the situation turns more complicated. We now observe the beam cores surrounded, more or less, by halo particles in all three cases. Each core is executing a rather large oscillation about uniform distribution in real space, which is the main cause of halo formation from rms-matched beams.

As long as we employ the concept of rms matching, it is generally impossible to avoid the plasma oscillations driven through the initial density-redistribution process. As an example, let us take a look at Fig. 5, in which the density evolution of an rms-matched Gaussian beam is demonstrated. We see that the core has been dominated by a significant breathing oscillation involving higher-order modes. To prevent this, we must start with the stationary state which

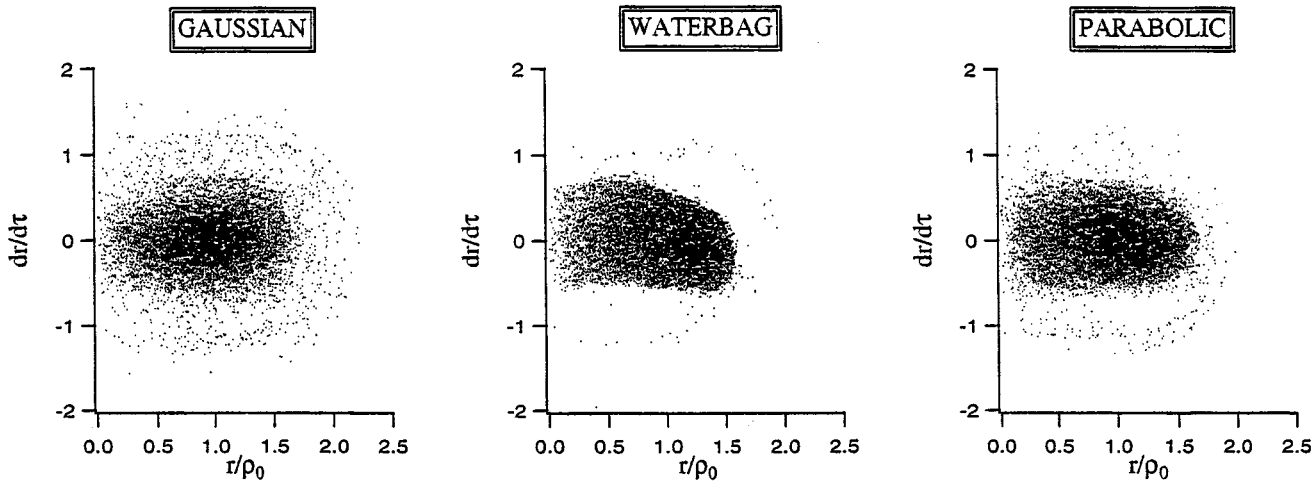

FIG. 4. Phase-space configurations of rms-matched beams with $\eta=0.3$ at $\tau/\tau_p=20$.

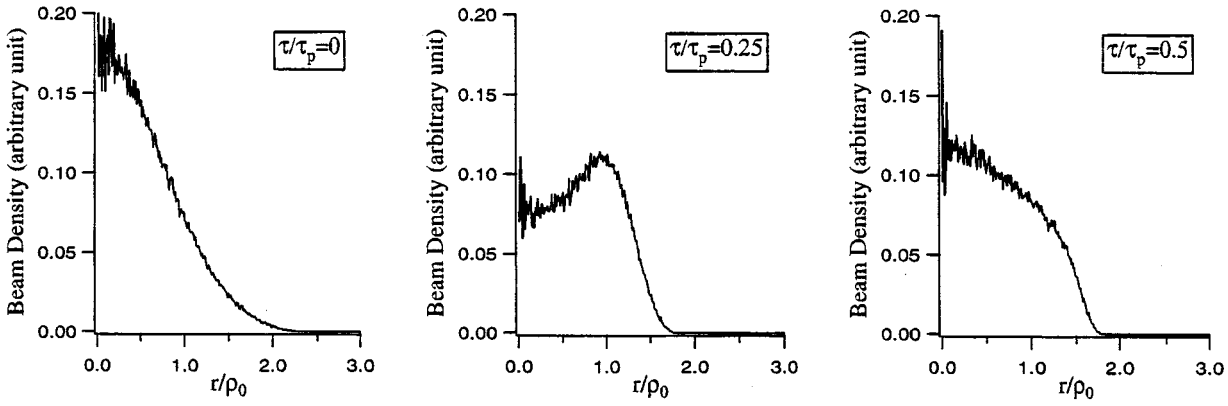

FIG. 5. Time evolution of the real-space density $n(r)$. The initial beam distribution is an rms-matched Gaussian with $\eta=0.3$.

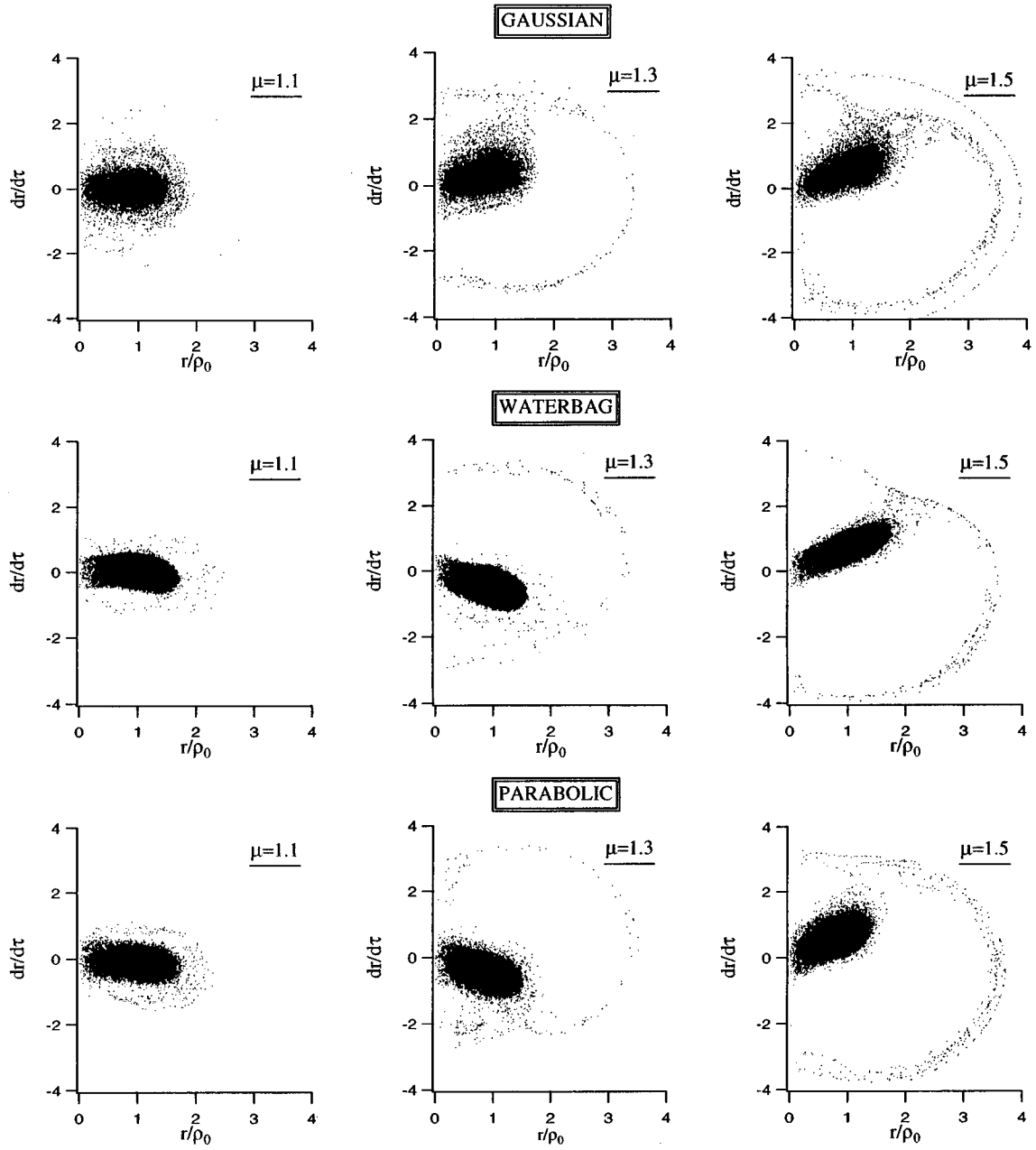

FIG. 6. Phase-space configurations of mismatched beams with $\eta=0.3$ at $\tau/\tau_p=20$. Three different initial mismatches, i.e., $\mu=1.1$, 1.3, and 1.5, have been applied to Gaussian, waterbag, and parabolic beam.

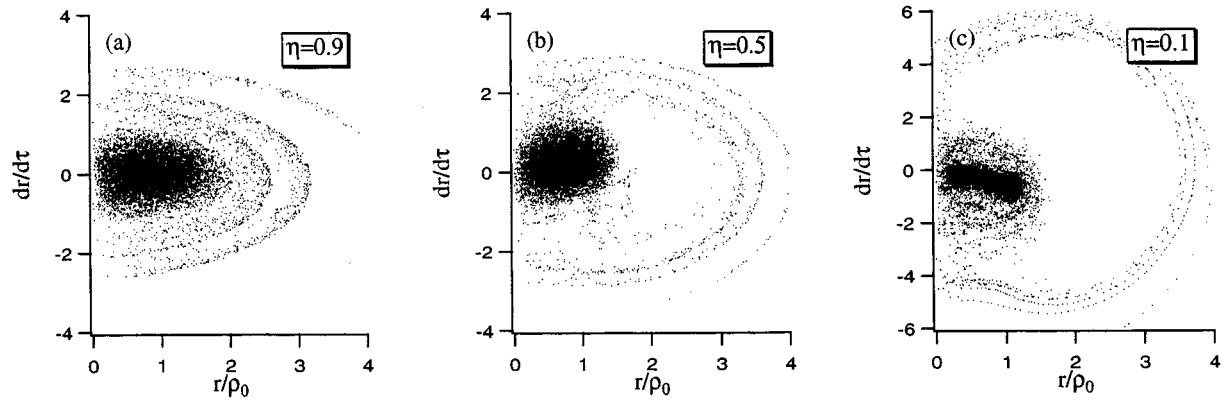

FIG. 7. Phase-space configurations of mismatched Gaussian beams with $\mu=1.5$ and $\tau/\tau_p=20$. Three different tune depressions, i.e., $\eta=0.9$, 0.5, and 0.1, have been considered. Note that the scale of ordinate is different in the $\eta=0.1$ case.

can be found by solving the Vlasov-Poisson equation system. However, initial distributions employed in simulation studies are usually defined with a linear Hamiltonian because of difficulty in getting a self-consistent solution to the Vlasov-Poisson equations. Then, as shown above, even an rms-matched beam can produce a halo when the density is high.

We now go to mismatched situations. Three different mismatch factors have been tried to obtain Fig. 6, where phase-space configurations at $\tau/\tau_p=20$ are displayed. The tune depression assumed in these pictures is 0.3. Specifically, we observe halos with no exception. It is interesting that, in most cases, halo particles are not uniformly distributed around a core but travel along several specific orbits forming narrow bands. Clearly, this tendency is more strengthened as the size of initial mismatch becomes larger. Naturally, larger mismatch causes halo loops more expanded in radius.

Figure 7 is based on Gaussian beams having different densities but the same initial mismatch, i.e., $\mu=1.5$. Halo formation appears to be quite serious even for the low-density beam. It is worthwhile to note that, in the $\eta=0.1$ case, the core is surrounded not only by a usual halo ring but also by a low-density cloud localized near the core. While the maximum halo amplitudes have not changed much depending on the tune depression, the beam of the $\eta=0.1$ case has clearly been widened in the p_r direction in phase space, which leads to a particularly large emittance growth. This effect may be explained by the stochastic core instability observed in Fig. 2(b).

V. DISCUSSION

A. The origin of halo particles

To avoid confusion, we may first need to have a consensus about what the term *core* means. Actually, this term has sometimes been used to express the dense region of a beam in *real space*, but we do not accept this definition here since many halo particles can exist inside the real-space core at any time. Instead, we refer to the dense region in *phase space* as the beam core. It then becomes no problem to distinguish a core region from a halo, as we have seen in the simulation results given in Sec. IV.

A question arises, however; namely, do halo particles really keep staying outside the phase-space core? To answer this question, let us trace back the particles which have eventually formed a halo. As an example, we consider here the case in Fig. 8(a), which shows a mismatched parabolic beam having already been transported by the distance of $20\tau_p$. To separate the halo part of this beam, we check the maximum betatron amplitudes of individual particles, attaining Fig. 8(b). We then trace back the selected halo particles to figure out where they came from. This procedure results in Fig. 8(c) indicating that the halo is largely composed of the particles initially located in the tail region. We have verified, with a number of simulations, that the main body of a halo originates from the fringe portion of a phase-space distribution, which implies that the beam core is *roughly* stable even with a large mismatch.

This conclusion is further supported by the simulation result in Fig. 9, where we have taken only the core part of Fig. 8(a) as an initial beam; namely, we have started with the beam from which the particles in Fig. 8(b) have been removed. After traversing the transport system of $20\tau_p$ long, the core beam in Fig. 9(a) has come to the state in Fig. 9(b). We see that no halo has been regenerated, although the beam intensity has been reduced about 16% compared to the original beam in Fig. 8(a) due to the removal of the halo particles. In addition, the emittance growth has also been completely suppressed while in the final state, illustrated in Fig. 8(a), the rms emittance was almost twice as large as the initial value.

The observations above suggest a possibility of eliminating halo particles by means of a simple collimator system. One possibility is just to put a scraper of a finite length. It is obvious that a single momentary scraping does not work since it only takes away a portion of a halo. The required length of the scraper is the shortest, provided that a beam has already reached the final saturated state. However, to have a satisfactory scraping effect, it may have to be much longer than the half betatron period $\pi/\eta\kappa$ which could already be rather long for a dense beam. Moreover, in this halo-scraping scheme, we must be very careful about the effects of image charges induced on the scraper wall. The practicability of a long scraper may thus be uncertain.

An alternate, probably more promising, possibility is the use of thin but several tapered collimators periodically installed along the beam line. The tapering angle must be determined such that the effects of the geometrical wake, as

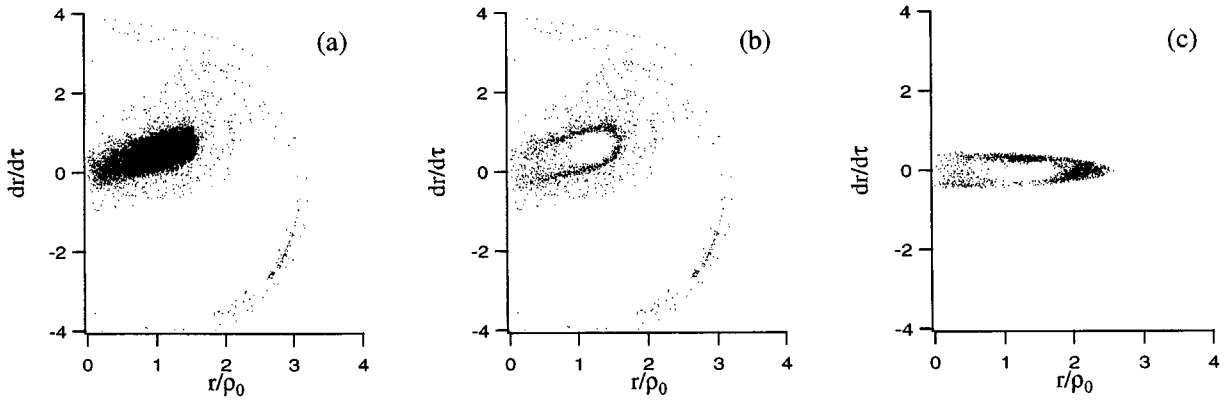

FIG. 8. Phase-space configurations of a parabolic beam with $\eta=0.2$ and $\mu=1.3$ initially. (a) represents the phase-space profile after the beam has been transported through a uniform channel of $20\tau_p$ long. Only the halo particles seen in (a) have been plotted in (b). Here, the particle which achieved a betatron amplitude greater than $1.3\times\sqrt{2}\rho_0$ has been defined as a halo particle. This corresponds to adopting $G=1.0$ where the parameter G is called *core factor*, introduced in Sec. V C. (c) shows the initial positions of the halo particles, obtained by back tracking the particles in (b). Pay attention to the fact that the core region in (b) is almost empty, which already implicates the core stability.

well as the resistive wall wake, are minimized. Though it is not very clear whether a halo can completely be removed by such a system, we could, at least, anticipate a significant reduction of the halo intensity. The required minimum number of thin collimators may be two; namely, the first collimator gets rid of about a half of a halo and, then, the second collimator installed some distance away from the first one scrapes most of the rest. But, to improve the efficiency of the system, we need to employ more than two collimators located a bit closer to each other. The multiple collimator system is of practical interest because of its simplicity, and should be studied further as a possible halo-scraping device.

B. The size of halo extent

From a practical viewpoint, it is important to know how far halo particles can be away from the beam center. According to our simulations, most initial beams come to a roughly saturated state before arriving at $\tau/\tau_p=20$, so we here consider the largest particle amplitude recorded until then to be the maximum beam extent. Further, for Gaussian beams, we initially truncate the tail particles at 3σ. Figure 10 shows the ratio of the maximum extent of halos from rms-matched beams to the radius of a matched KV beam, i.e., $\sqrt{2}\rho_0(\equiv R_0)$. It is recognized that the largest halo amplitude is not very sensitive to the beam density. Though all three types of distributions yield halos at $\eta=0.3$, as already demonstrated in Fig. 4, the corresponding maximum beam extents are comparable to those in the lower-density region where no remarkable halos have been developed. This implies that halo formation is not troublesome when a beam is initially rms matched.

The slight distribution dependence of halo size indicated in Fig. 10 is not of essential importance since it simply arises from the discrepancy of the initial beam-boundary sizes (compare, for example, the upper pictures in Fig. 3). In fact, if we take the ratio to initial beam radius instead of $\sqrt{2}\rho_0$, the result becomes much less dependent on beam distributions. We then find that the growth rate of the beam boundary is mostly less than about 10% for all three distributions even in a high-density region.

For mismatched beams, we obtain Fig. 11 where the ordinate indicates the maximum halo size divided by $\mu\sqrt{2}\rho_0$. We again notice that there exists no clear correlation between the scaled halo extent and tune depression. It is quite interesting that even the distribution dependence of the halo extent has disappeared when the magnitude of the initial mismatch exceeds some level. We can directly confirm this fact by looking at the phase-space configurations in Fig. 6. While

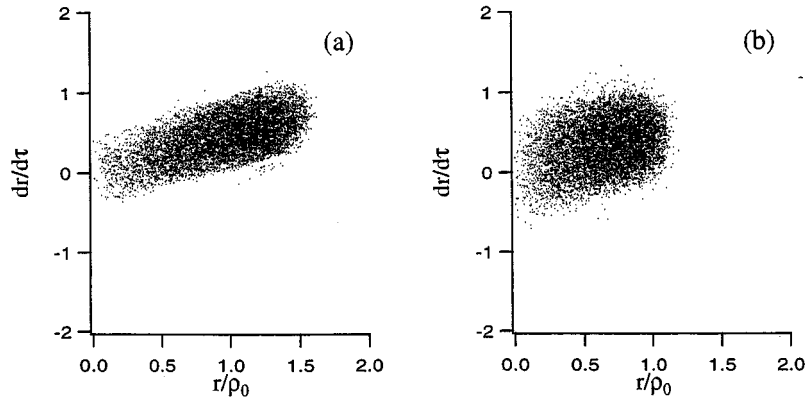

FIG. 9. Phase-space configurations of a core beam. (a) shows the initial beam obtained by removing the halo particles in Fig. 8(b) from the original beam in Fig. 8(a). After traveling through a uniform channel of $20\tau_p$ long, the core beam in (a) reaches the distribution in (b).

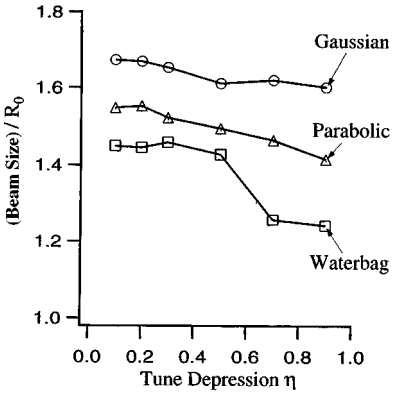

FIG. 10. Maximum beam extent vs tune depression (rms-matched case). The ordinate indicates the ratio of maximum halo extent to the radius of matched KV core $R_0=\sqrt{2}\rho_0$.

the halos have been more enlarged in Fig. 6 with increasing initial mismatch, we may now state, based on the information provided by Fig. 11, that it is simply because the halo extent scales as μ when μ is sufficiently above one. The universality of the maximum beam size pointed out in Figs. 11(b) and 11(c) leads us to the conclusion that the possible halo extent should be, at most, approximately 2μ times the matched KV-beam size $\sqrt{2}\rho_0$ regardless of beam density.

C. The intensity of halo current

The approximate stability of the beam core confirmed in Sec. V A allows us to estimate the intensity of the halo current. To separate a halo part from a core part, we here set the circular boundary in real space whose radius is $r=G\mu\sqrt{2}\rho_0$, where we call the parameter G *core factor*. Once a particle goes beyond this boundary, we simply regard it as a halo particle. Note, however, that we should not initiate this procedure until the density-redistribution process is completed. Otherwise, particles initially located near the beam edge in real space may inevitably be counted as halo particles, leading to an overestimation of the halo current. Once initial beams have been redistributed to possess a nearly uniform density, it then becomes unnecessary to worry, at least, about the possibility of such overestimation. Since beam density is known to be very quickly homogenized, we start here marking halo particles after a beam travels through the channel by a distance of $5\tau_p$.

The halo intensities evaluated with the above-explained method are demonstrated in Fig. 12, where the upper three pictures correspond to the $G=1.2$ cases, the middle three to the $G=1.3$ cases, and the lower three to the $G=1.4$ cases. The pictures on the left side, i.e., the $\mu=1.1$ case, clearly show the natural tendency that halo intensity becomes smaller for a larger core factor. When $G=1.2$, it appears, against expectation, that halos have been more enhanced in a lower-density region rather than in a higher-density region. This is, however, largely due to the simple fact that a beam core is more expanded in radius at a lower density.

The middle and lower pictures of the $\mu=1.5$ case look roughly analogous to each other, which implicates that the maximum radii of the strongly mismatched cores should typically be less than around $1.3\mu\sqrt{2}\rho_0$, while they could be somewhat altered, depending on the density. The average amount of a halo over the whole density region has been calculated, in the $\mu=1.5$ case, to be 9.3% ($G=1.2$), 8.2% ($G=1.3$), and 7.3% ($G=1.4$) for Gaussian beams, 6.4% ($G=1.2$), 5.9% ($G=1.3$), and 5.7% ($G=1.4$) for parabolic beams, and 5.1% ($G=1.2$), 2.9% ($G=1.3$), and 2.7% ($G=1.4$) for waterbag beams.

The halo intensity evaluated with a specific core factor should be of practical importance, since we generally care about the real-space oscillation amplitudes of individual particles either when designing a halo scraper or when deciding the minimum aperture size of a linac. It might, however, be meaningful to evaluate the intensity of only the halo portion, taking into account the density dependence of the core size mentioned above. Figure 13 gives the result of the rough estimate of halo intensity obtained by adjusting the value of G. We now realize that a larger mismatch has caused a beam to generate a more serious halo. Further, it seems that the halo has been more enhanced at a higher density, while this tendency has been weakened as the density becomes lower. In particular, above around, say, $\eta=0.5$, no explicit correlation between halo current and tune depression is visible. Figure 13 also tells us that the waterbag distribution is relatively stable compared to the other two distributions. In fact, even

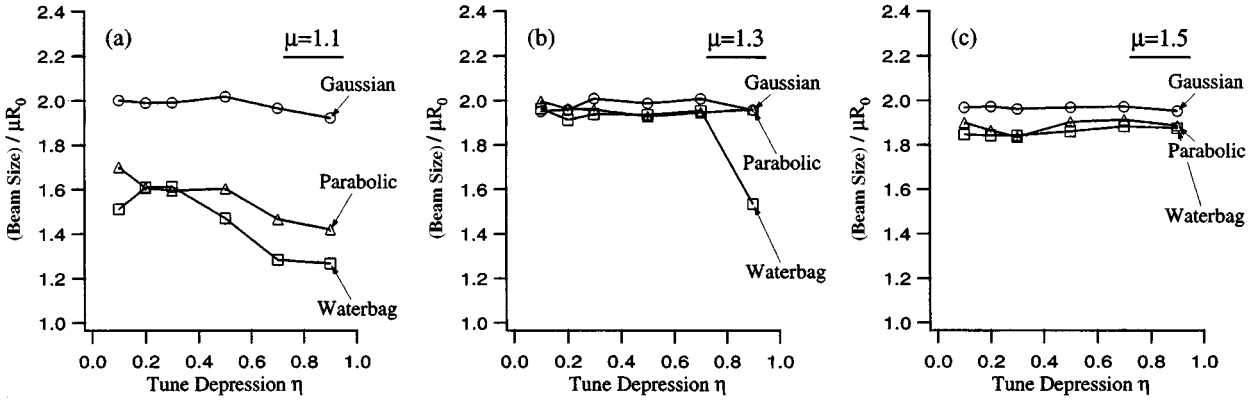

FIG. 11. Maximum beam extent vs tune depression (mismatched case). The ordinate indicates the ratio of maximum halo extent to the maximum radius of a mismatched KV core, i.e., $\mu\sqrt{2}\rho_0$.

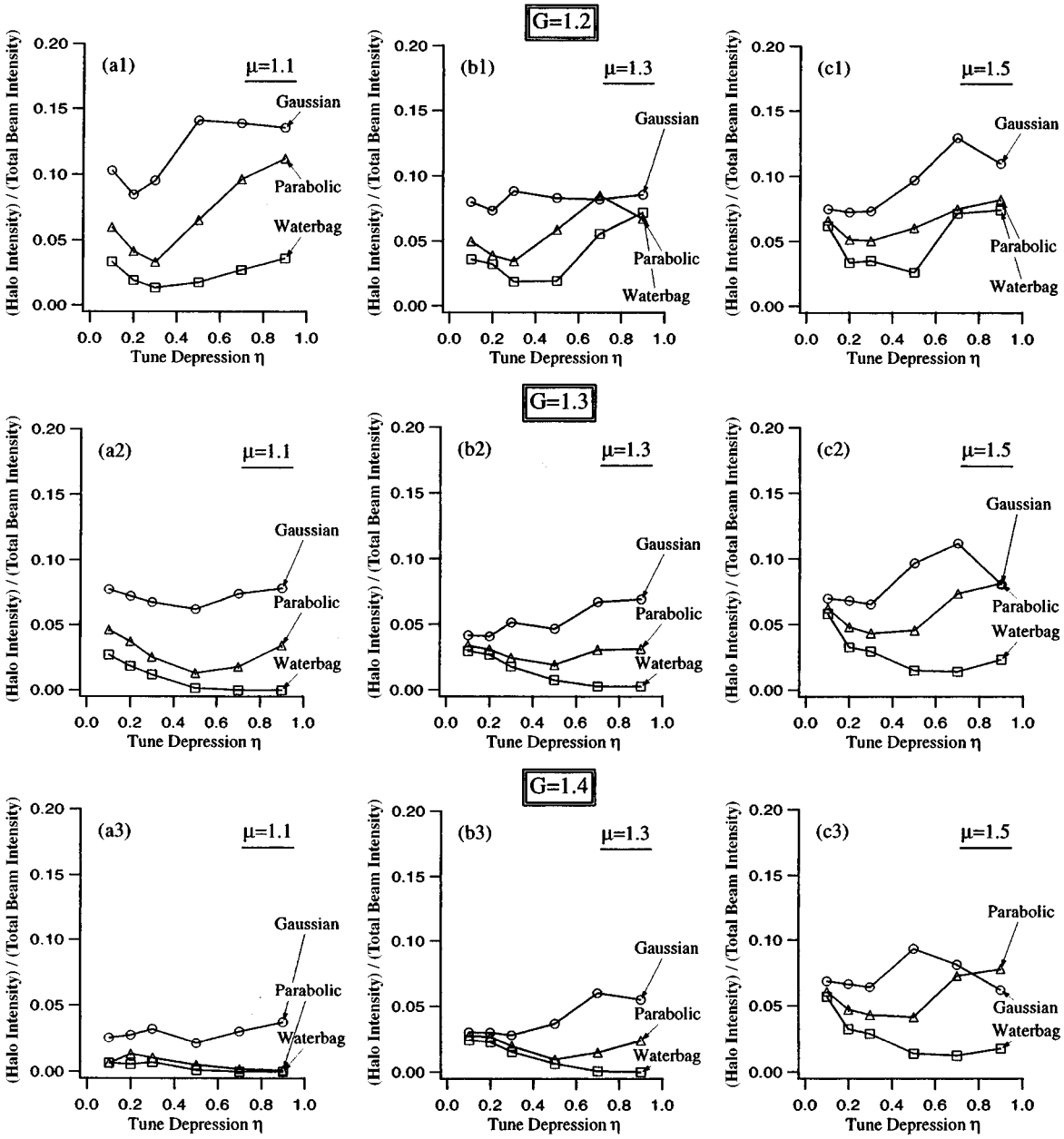

FIG. 12. Halo intensity relative to total beam intensity vs tune depression. Halo intensity has been evaluated at $\tau/\tau_p = 20$ with various core factors and mismatch factors.

with a mismatch factor of 1.5, only less than 10% emittance growth, due to halo formation, took place in waterbag beams when the density was modest. A key factor in explaining this distribution dependence may be the difference of the nonlinear field energies involved in initial beams. As analyzed in previous works, the nonlinear field energy of a waterbag beam is much smaller than those of the other two beams (see, e.g., Ref. [11]). Among the three distributions, the Gaussian has the largest nonlinear field energy; namely, about seven times larger than the waterbag, and about three times larger than the parabolic. This may be why halos from Gaussian beams are always most predominant.

Finally, it is important to note that there may be a possibility of observing halos produced by the same mechanism as described here, even in a circular ion machine. In fact, we have confirmed the formation of a remarkable halo even in the $\eta = 0.99$ case provided that the mismatched is large.

VI. SUMMARY

As far as cylindrical beams propagating in a uniform focusing channel are concerned, the deviation of beam distribution from the stationary state may be understood as the main cause of halo formation. Whenever a beam is not in its own stationary state, it naturally tries to approach closer to there, minimizing the nonlinear field energy. During this process, plasma oscillations are excited in the beam core, driving a portion of it into a halo. Inversely speaking, if a beam injected into a uniform channel is *fine grainedly* matched to it, there is no reason to expect the development of a halo unless the distribution itself is intrinsically unstable against perturbation. While several different factors have been con-

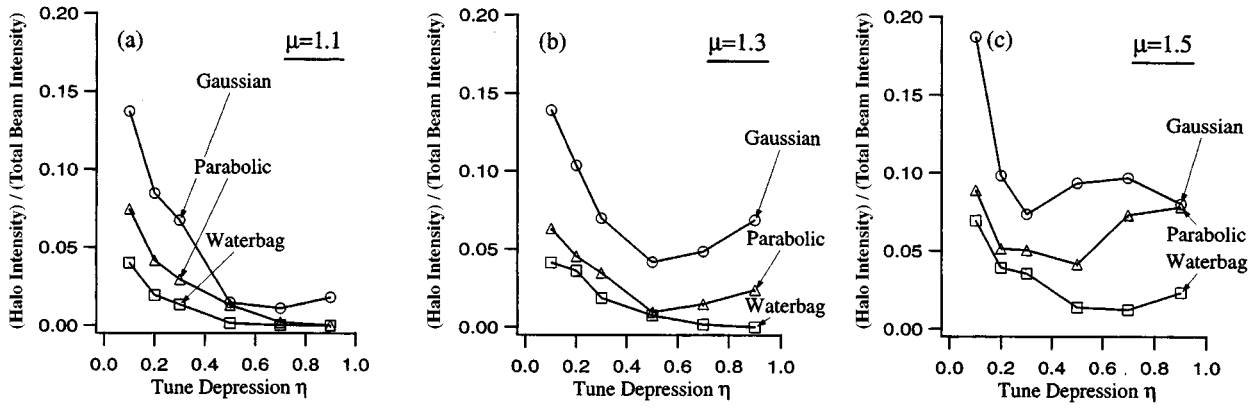

FIG. 13. Halo intensity relative to total beam intensity vs tune depression. Halo intensity has been evaluated at $\tau/\tau_p = 20$. The core factor has been modulated taking into account the density dependence of core radius; namely, a smaller value of core factor is usually adopted at a higher density since a core is more strongly homogenized. Note that halos have been considerably enhanced in a very high-density region due to the existence of the particle cloud around a core [see Fig. 7(c)]. If we neglect the contribution from this cloud, the halo intensities at $\eta = 0.1$ are reduced to the 10% level or less.

sidered as the possible sources of halo formation, it seems, after all, that the important point is how much a beam is deviated from the stationary state [20].

According to the present simulations, a beam core defined in phase space is approximately stable regardless of its density and the size of mismatch. Most parts of a halo are thus formed by the particles moving outside the core boundary. This means that we do not have to care too much about the mechanism which enables some ions to escape from the core. The particle-core approach might, therefore, be helpful in exploring some features of halos although it definitely has limitations.

Figure 13 suggests that a beam with a larger mismatch yields a more dominant halo. Moreover, it also appears that halo intensity becomes less dependent on tune depression in a lower-density region. While the absolute amount of halo particles changes associated with the beam distribution, it could be around 5% or more of the total particle number either when an initial beam is subjected to a large mismatch or when the beam density is extremely high. However, due to the approximate stability of the phase-space core, we have a possibility of removing a large portion of the halo ring surrounding the core, for example, by means of a multicollimator system.

It has also been discovered that the maximum extent of halos normalized with ρ_0 are surprisingly insensitive to the tune depression η. In particular, the maximum halo size of a Gaussian beam divided by its initial rms radius is independent of both the beam density and mismatch factor; namely, it always takes a value around $2\sqrt{2}$ as indicated in Fig. 11. Concerning the other two beam distributions, the maximum beam radii tend to be closer to that of the Gaussian case as the degree of the initial mismatch increases. It may then be concluded that the minimum aperture radius of a high-intensity linear machine must be greater than, at least, $2\mu_{\max}$ times the matched KV-beam radius $\sqrt{2}\rho_0$, when one expects the possible maximum mismatch to be $\mu_{\max}$.

ACKNOWLEDGMENT

The authors would like to thank Dr. K. Hirata and Dr. K. Oide for useful discussions.

[1] M. Reiser, in *Proceedings of the Particle Accelerator Conference, San Francisco, 1991* (IEEE, New York, 1991), p. 2497; A. Cucchetti, M. Reiser, and T. Wangler, *ibid.*, p. 251; D. Kehne, M. Reiser, and H. Rudd, in *Proceedings of the Particle Accelerator Conference, Washington, D.C., 1973* (IEEE, New York, 1993), p. 65.

[2] R. A. Jameson (unpublished).

[3] *Heavy Ion Fusion*, edited by M. Reiser, T. Godlove, and R. Bangerter, AIP Conf. Proc. No. 152 (AIP, New York, 1986).

[4] R. A. Jameson, Los Alamos Report LA-UR-93-1029, 1993 (unpublished).

[5] R. L. Gluckstern (unpublished); Phys. Rev. Lett. **73**, 1247 (1994).

[6] J. S. O'Connell, T. P. Wangler, R. S. Mills, and K. R. Crandall, in *Proceedings of the Particle Accelerator Conference, Washington, D.C., 1993*, Ref. [1], p. 3657.

[7] J. M. Lagniel, Nucl. Instrum. Methods A **345**, 46 (1994); **345**, 405 (1994).

[8] A. Riabko *et al.*, Phys. Rev. E **51**, 3529 (1995).

[9] I. M. Kapchinskij and V. V. Vladimirskij, in *Proceedings of the International Conference on High Energy Accelerators* (CERN, Geneva, 1959), p. 274.

[10] R. L. Gluckstern (unpublished); it is not obvious whether the stability of the linear breathing mode is guaranteed when the size of an initial mismatch can no longer be treated as perturbation. However, in the particle-core model, we simply assume that a KV core executes a stable linear breathing oscillation in spite of a large mismatch.

[11] J. Struckmeier, J. Klabunde, and M. Reiser, Part. Accel. **15**, 47 (1984); O. A. Anderson, *ibid.* **21**, 197 (1987).

[12] Needless to say, this sentence does not mean that the particle-core model gives us an exact picture of the halo formation mechanism. For instance, the core separatrix of a realistic beam, if we can rigorously define such a boundary, must definitely be different from that of a KV beam. In fact, as pointed out in Sec. II, the nonlinearly of a realistic beam may even partly destroy the core stability, yielding a stochastic region around the shrunk core.

[13] F. J. Sacherer, IEEE Trans. Nucl. Sci. **NS-18**, 1101 (1971).

[14] C. Chen and R. C. Davidson, Phys. Rev. E **49**, 5679 (1994); Phys. Rev. Lett. **72**, 2195 (1994).

[15] S. Y. Lee and A. Riabko, Phys. Rev. E **51**, 1609 (1995).

[16] In the present paper, we only consider mismatch factors greater than one.

[17] Note that the phase-space distribution of a KV beam is quite different from that of a more realistic beam even if both have similar density profiles in real space.

[18] The maximum allowable value of μ is limited in this model because of the assumption made. For example, in order for Eqs. (2.9) and (2.11) to have a physical solution, μ must be less than about 1.15 when $\eta = 0.5$.

[19] The stationary distribution of a dense beam is roughly uniform in real space. Whenever the beam is deviated from the stationary state, it tries to approach closer to there, homogenizing its real-space density. The density redistribution process should thus have essentially nothing to do with resonances nor chaos. See, e.g., Ref. [11] or the excellent work by T. P. Wangler *et al.*, IEEE Trans. Nucl. Sci. **NS-32**, 2196 (1985) which has been generalized by I. Hofmann and J. Struckmeier, Part. Accel. **21**, 69 (1978).

[20] When the external restoring force varies periodically, the situation may become different as the envelope of even a fine-grained matched beam can execute a large oscillation. It is not very clear whether a matched beam in a periodic channel exhibits the dynamical behavior analogous to that of a mismatched beam in a uniform channel. This problem will be discussed in detail in a forthcoming paper.

[21] Waterbag core has a uniform particle distribution in phase space.